POLISH MARITIME RESEARCH Special Issue 2017 S3 (95) 2017 Vol. 24; pp. 123-129
10.1515/pomr-2017-0114

INVESTIGATIONS OF TOPOGRAPHIC EFFECT ON RADIAL CURRENT IN SOUTH YELLOW SEA

Cheng Chen[1,*]
Yigang Wang[2]
Huiming Huang[2]
[1] College of Civil Engineering, Fuzhou University, Fuzhou 350116, China
[2] College of Harbor, Coastal and Offshore Engineering, Hohai University, Nanjing 210098, China
* corresponding author

ABSTRACT

Large scaled projects are conducted in South Yellow Sea in recent years. Topographic effect and tidal current are key issues to the coastal engineering and the ocean engineering. In this study, field surveys were conducted to investigate the tidal level, current velocity, and current direction in South Yellow Sea. A numerical model was developed to simulate the radial current field based on the field data. To investigate the mechanism of the radial current field, the actual topography and a smoothed topography were applied in the numerical model, respectively. Results show that, the current field appeares radial because of the tidal system rather than the submarine topography. Local topography centralized the radiation centre and shifted the high-velocity zones. The actual topographic effect is proposed, and results show that local topography increases the flood tide velocity and decreases the ebb tide velocity. Lagrangian residual currents are calculated to illustrate possible sediment sources and transport routes.

Keywords: Field survey; Numerical model; Topography; Radial current; Lagrangian residual current

INTRODUCTION

The sand ridges are formed due to the interactions of tidal currents and sediments [1], and further shaped by waves [2]. The coast of Eastern China includes more than 10 large sand ridges [3], which will be reclaimed before 2020 [4]. However, there is a radial current field in the coast of Eastern China, which makes reclamation project need to be investigated.

To have a better understanding of this current field, some numerical works have been done by researchers. Xia et al. [5] simulated the M2 tide in the Yellow Sea, using 20 km computational grids to smoothed the detailed topography. The results showed that the radial tidal currents still exist in this study area even using such coarse computational grids. Zhu et al. [6] established a 2-D tidal current model using finer computational grids (10 km) with an approximately rectangular coastline. It was also found that the radial current field was not generated by marine topography. Further considering tidal currents, waves and storm surges in the numerical simulation, Zhang et al. [7] explained how the radial sand ridge topography had been forming and evolving, i.e. tidal current-induced formation, storm-induced change, tidal current-induced recovery. The radial current field has existed for thousands of years [8, 9], providing sufficient time to generate the sand ridge topography. Zhang et al. [8] conducted numerical experiments on the propagation of M2 tidal wave in ancient coast conditions and generated the similar tidal wave system as present. Zhu [9] established a 2-D numerical model for tidal current research in Bohai Sea, Yellow Sea and East China Sea to simulate the tidal current in 7000a B.P. and 3800a B.P.. The results showed that a standing tidal wave system existed solitarily at both 7000a B.P. and

3800a B.P., respectively. Besides, the radial tidal current field has been in Jiangsu coastal area since maximum marine transgression in the last glacial age, i.e. there is no obvious change with the coastline variation. The local tidal currents are also influenced by the sand ridge topography. Chen et al. [10] showed that, the sand ridges are migrating southward due to the large-scaled hydrodynamic effect, and the current velocity tends to increase in the waterways between sand ridges. Xing et al.'s [11] numerical model indicated the erosion occurred in deep channels and the accretion occurred in shallow ridges. The previous discussions on the variation of sand ridge suggest that the sand ridge is the results of the radial current system over thousands of years.

In this study, a series of large-scaled field surveys were conducted and the data were used to validate the 2-D large-scaled hydrodynamic model in this study. This study was supportive to the provious findings on radial current fields. The current fields were simulated using gradually changing (smoothed) topography and actual (sand ridge) topography, respectively. Actual Topographic effect (ATE) is proposed as the difference between flow with and without sand ridge, to investigate the topographic effect on current field. The results from this numerical model proposed possible hydrodynamic explanations of the sediment sources and sediment transport routes.

MATERIAL AND METHODS

FIELD DATA COLLECTION

In this field survey, 14 stations were distributed in the study area (shown in Figure 1). Eight stations conducted suveys during both the spring tide and neap tide; another six stations conducted surveys during the spring tide.

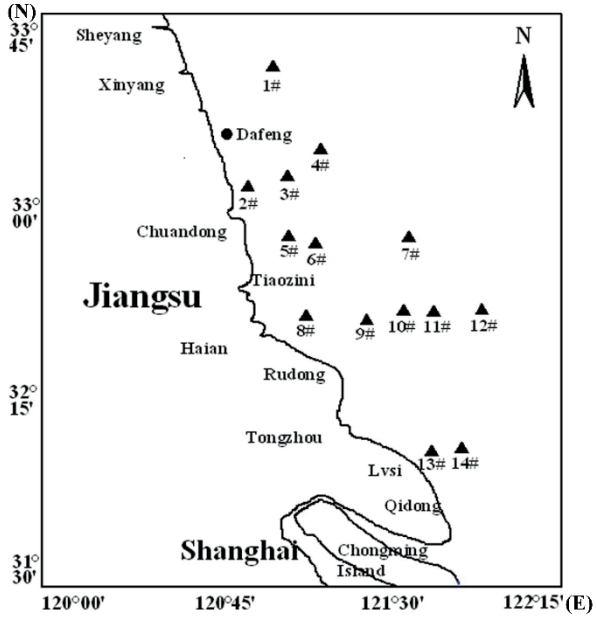

Fig. 1. Locations of the survey stations

Table 1 shows the detailed information for each survey station. The time-histories of tidal levels, current velocities and current directions were recorded in this field study. In addition, a long-term survey was conducted at Dafeng Port to record the time-history of tidal levels fozr 12 months. The stations cover most part of the South Yellow sea.

Tab. 1. Information of the survey stations

Stations	Latitude/(°N)	Longitude/(°E)	Survey period	Approximate position
1#	33.66	120.97	Spring tide	Outer Xingyang Port
2#	33.17	120.86	Spring tide & Neap tide	North of Chuandong Port
3#	33.18	120.91	Spring tide	North of Chuandong Port
4#	33.33	121.23	Spring tide & Neap tide	Outer Wang Port
5#	32.97	120.97	Spring tide & Neap tide	South of Chuandong Port
6#	32.90	121.05	Spring tide	South of Chuandong Port
7#	32.95	121.54	Spring tide & Neap tide	East of Chuandong Port
8#	32.58	121.15	Spring tide & Neap tide	Outer Xiaoyangkou Port
9#	32.55	121.33	Spring tide	Outer Xiaoyangkou Port
10#	32.66	121.50	Spring tide & Neap tide	East of Xiaoyangkou Port
11#	32.66	121.62	Spring tide	East of Xiaoyangkou Port
12#	32.66	121.75	Spring tide	East of Xiaoyangkou Port
13#	32.08	121.74	Spring tide & Neap tide	Outer Lvsi Port
14#	32.09	121.81	Spring tide & Neap tide	Outer Lvsi Port
Dafeng	33.28	120.80	12 months	Dafeng Port

The short-term survey for each individual station started at its local low tide. The initial recording times for all stations were different. This is because in this study area, local tidal wave phases at different stations were not exactly the same. In general, the recording lasted for approximately 27 hours, covering the one tidal cycle. To capture the current variations, samples were taken in 30 minute intervals during the maximum flood and the ebb period. During the rest of the time, samples were taken in 60 minute intervals. Table 2 shows the detailed recording periods for each survey station.

Tab. 2. Recording periods for each station

Sub-area	Spring tide			Neap tide		
	Survey Station	Start Time	End Time	Survey Station	Start Time	End Time
Xingyang Port	1#	17:00 Jan. 3	19:00 Jan. 4			
Wang Port	4#	18:00 Jan. 3	19:00 Jan. 4	4#	5:00 Jan. 11	7:00 Jan. 12
Chuandong Port	2#, 3#, 5#, 6#	17:00 Jan. 3	13:00 Jan. 4	2#, 5#	5:00 Jan. 11	7:00 Jan. 12
Outer Chuandong Port	7#	17:00 Jan. 3	19:00 Jan. 4	7#	5:00 Jan. 11	7:00 Jan. 12
Xiaoyangkou & Lvsi Port	8#, 9#, 10#, 11#, 12#, 13#, 14#	17:00 Jan. 3	21:00 Jan. 4	8#, 10#, 13#, 14#	5:00 Jan. 11	7:00 Jan. 12

Roundtrip measurements were applied in the field surveys to increase the accuracy of the data. If the water is deeper than 5 m, six-point sampling method was adopted along the vertical profile. If the water is shallower than 5 m, three-point sampling method was adopted instead. In the two-dimensional numerical model, the current velocities were validated by the field data of mean velocitied calculated from the vertical profile. The major devices and instruments for the survey are listed in Table 3.

Tab. 3. Main devices for field surveys

Instruments	Type	Application
GPS Receivers	Trimble 4700	Positioning System
Beacon Receivers	Trimble DSM212	Hydrological Measurement
Hand-held GPS	Garmin 12xlc	Investigation System
Navigation Software	HYPACK(V8.1a)	Navigation Data Acquisition
Flow Velocity Instrument	ZSX-III Series	Current Data Collection
Others	Current Meter, Anemorumbo meter, Hydrographic Winch, Fish Lead, Laptop, Electric Generator, Wireless interphone, etc.	

NUMERICAL MODEL

In this study, a numerical model MIKE21 was used and validated based on field data. DHI's Software contains a modelling system for estuaries, coastal waters and seas. Therefore, a two-dimensional model was built within the commercial MIKE 21 FM package to simulate tidal hydrodynamics in the study area. The main governing equations are the continuity equation and the incompressible Reynolds-averaged Navier-Stokes (RANS) equations. The N-S equations are used based on the static pressure hypothesis and Boussinesq hypothesis. The vertical current acceleration is ignored compared to the gravity acceleration, and the turbulence stress is with respect to the time averaged velocity gradient. The basic equations to describe tidal hydrodynamics can be written as:

$$\frac{\partial h}{\partial t}+\frac{\partial h\bar{u}}{\partial x}+\frac{\partial h\bar{v}}{\partial y}=hS \tag{1}$$

$$\frac{\partial h\bar{u}}{\partial t}+\frac{\partial h\bar{u}^2}{\partial x}+\frac{\partial h\bar{u}\bar{v}}{\partial y}=f\bar{v}h-gh\frac{\partial \eta}{\partial x}-\frac{h}{\rho_0}\frac{\partial P_a}{\partial x}-\frac{gh^2}{2\rho_0}\frac{\partial \rho}{\partial x}+\frac{\tau_{sx}}{\rho_0}-\frac{\tau_{bx}}{\rho_0}-\frac{1}{\rho_0}\left(\frac{\partial S_{xx}}{\partial x}+\frac{\partial S_{xy}}{\partial y}\right)+\frac{\partial}{\partial x}(hT_{xx})+\frac{\partial}{\partial y}\left(hT_{xy}\right)+hu_sS \tag{2}$$

$$\frac{\partial h\bar{v}}{\partial t}+\frac{\partial h\bar{u}\bar{v}}{\partial x}+\frac{\partial h\bar{v}^2}{\partial y}=-f\bar{u}h-gh\frac{\partial \eta}{\partial y}-\frac{h}{\rho_0}\frac{\partial P_a}{\partial y}-\frac{gh^2}{2\rho_0}\frac{\partial \rho}{\partial y}+\frac{\tau_{sy}}{\rho_0}-\frac{\tau_{by}}{\rho_0}-\frac{1}{\rho_0}\left(\frac{\partial S_{yx}}{\partial x}+\frac{\partial S_{yy}}{\partial y}\right)+\frac{\partial}{\partial x}\left(hT_{xy}\right)+\frac{\partial}{\partial y}\left(hT_{yy}\right)+hv_sS \tag{3}$$

where x and y are horizontal Cartesian coordinates; η is the surface elevation; t is time; h is the total water depth; $\bar{u}$ and $\bar{v}$ are depth-averaged velocity components in x and y directions, respectively; P_α is the local atmospheric pressure; ρ_0 is the reference of water density; ρ is the density of water; f is the Coriolis parameter; S_{xx}, S_{xy}, S_{yx}, S_{xz}, S_{yy} are components of radiation stress tensor; T_{xx}, T_{xy}, T_{yx} are the lateral stress including viscous friction, turbulent friction, and differential advection; (τ_{sx}, τ_{sy}) and (τ_{bx}, τ_{by}) are the components of wind stress and bottom stress, respectively; S is magnitude of point source discharge.

The model domain was established in a large-scaled area to provide a relatively accurate tidal wave system. The model boundaries were from 23°N northwards to the Asian continent coastline, and 128.5°E westwards to the Asian continent coastline (shown in Figure 2). The simulation time was from 8:00 30/12/2006 to 8:00 12/01/2007, which covered the spring tide period (from 17:00 03/01/2007 to 19:00 04/01/2007) and neap tide period (from 5:00 11/01/2007 to 7:00 12/01/2007). The study area was self-nested in the large-scaled model, which was from 31.8°N northwards to 34.2°N, and 122.8°E westwards to the Asian continent coastline. The actual (sand ridge) topography data and gradually changing (smoothed) topography data were used in the model, respectively. Therefore, two sets of corresponded current fields were simulated using the same hydrodynamic model setup except for the topography.

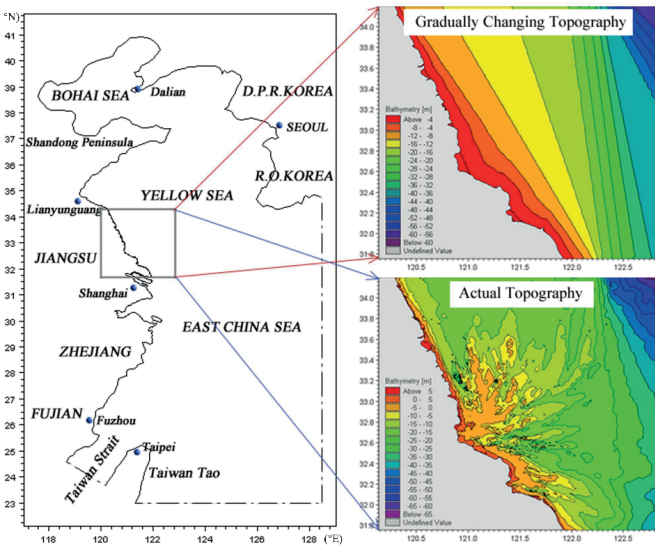

Fig. 2. Numerical model domain and topography in study area

The overview of the computational grids is shown in Figure 3. The unstructured grids were applied in the numerical model, and the grid sizes were changable. The coarser computational grids (larger than 10 km) were applied in the large-scaled model to reduce the computation work, while finer computational grids (less than 1 km) were applied in the self-nested area to provide relatively accurate modelling results.

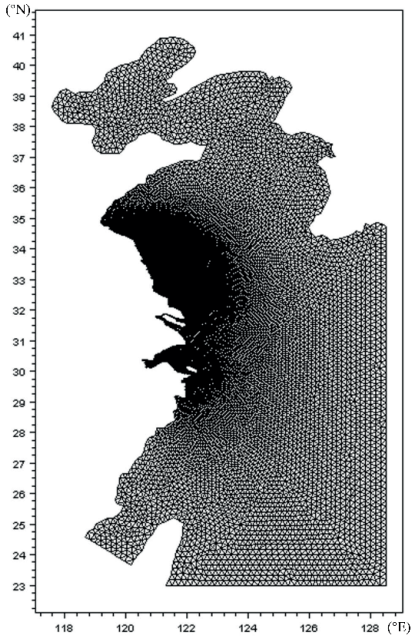

Fig. 3. Overview of the computational grids

The field data (including time-histories of tidal levels, current velocities and current directions) were collected to validate this numerical model. Figure 4 shows the time-history of the tidal levels for Dafeng Port as an example. The horizontal axis is the time (in hour). The initial time (0) stands for 17:00 03/01/2007, which is the beginning of the spring tide. Results of the tidal level indicate that the agreement between the measured value and simulated value is good.

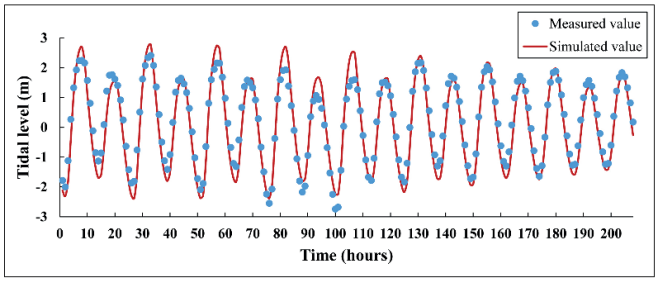

Fig. 4. Time-history of tidal level for Dafeng Port

Figure 5 shows the time-history of current velocities and directions for Lvsi Port (13# in Figure 1) as an example. The initial time (0) for Figure 5(a) and Figure 5(b) stands for 17:00 03/01/2007 (the beginning of the spring tide); the initial time for Figure 5(c) and Figure 5(d) stands for 05:00 11/01/2007 (the beginning of the neap tide). Good agreements were observed between the measured values and simulated values. Therefore, this hydrodynamic model was applied to study the current field, and two parallel experimental results from actual topography and gradually changing topography were compared and discussed. Results of the currents indicate that good agreement was observed between measured value and simulated value, and the numerical model has reliable results in current fields.

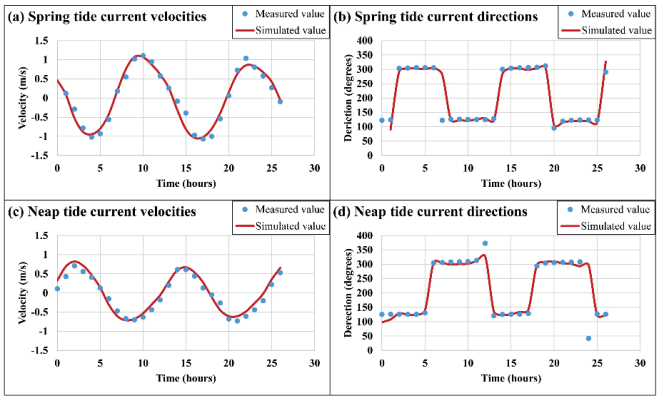

Fig. 5. Time-histories of current velocities and directions in for Lvsi Port (13# in Figure 1)

RESULTS AND DISCUSSIONS

CURRENT FIELDS AND MAXIMUM VELOCITIES

Figure 6(a) and Figure 6(b) present the radial current field on two topographies during flood period, and Figure 6(c) and Figure 6(d) are the ones during ebb period. The horizontal axis is the longitude (in °E), and the vertical axis is the latitude (in °N). The results indicated the radial

current field was not generated by the actual (sand ridge) topography since it also existed on the gradually changing (smoothed) topography. Numerical model results also showed the moving progress of the tidal wave. It was observed that there are two tidal waves in this study area, i.e. a progressive tidal wave propagating from the southeast towards the Yellow Sea, and a counter-clockwise rotary tidal wave reflected by the Shangdong Peninsula. These two tidal waves converged as a dual-tide system and generated a unique radial current field.

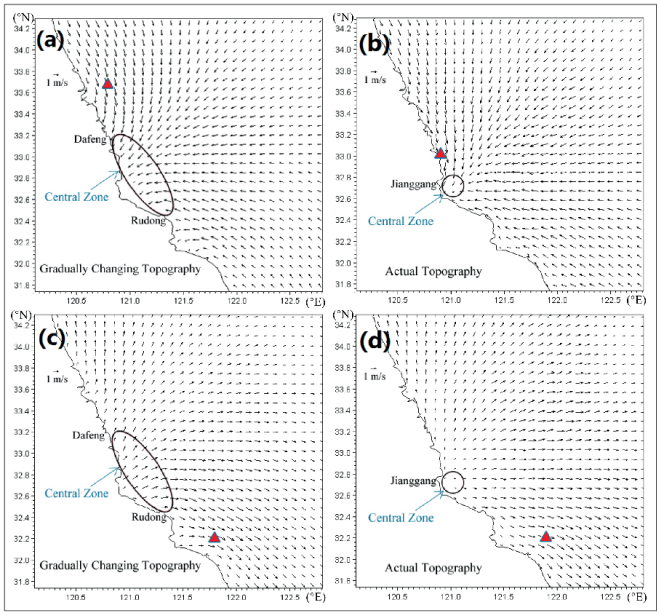

Fig. 6. Radial current field in study area. (a) gradually changing topography during flood tide pe-riod; (b) actual topography during flood tide period; (c) gradually changing topography dur-ing ebb tide period; (d) actual topography during ebb tide period

However, the actual (sand ridge) topography still demonstrated some effects on current field: 1) it narrowed the centre zone of the radial current field; 2) it increased the maximum flood velocity from 1.75 m/s to 2.19 m/s, and decreased the maximum ebb velocity from 1.66 m/s to 1.61 m/s; 3) it shifted the strongest flood point for approximately 73 km, from (120°49'27"E, 33°40'19"N) to (120°53'54"E, 33°0'45"N), and shifted the strongest ebb point for approximately 11 km, from (121°47'23"E, 32°10'47"N) to (121°54'31"E, 32°10'14"N).

ACTUAL TOPOGRAPHIC EFFECT (ATE)

The ATE is proposed herein to better investigate the actual (sand ridge) topographic effect on current field. VTE is expressed as follows:

$$\vec{A}_{ij} = (u_{aij} - u_{gij}, v_{aij} - v_{gij}) \quad \textbf{(4)}$$

where $\vec{A}_{ij}$ is a vector indicating the actual topographic effect at position (i, j); u_{aij} is the horizontal component of actual topography current velocity at position (i, j); u_{gij} is the horizontal component of gradually changing topography current velocity at position $((i, j)$; v_{aij} is the vertical component of actual topography current velocity at position $((i, j)$; v_{gij} is the vertical component of gradually changing topography current velocity at position $((i, j)$. Figure 7 shows the unit ATE in the study area. The horizontal axis is the longitude (in °E), and the vertical axis is the latitude (in °N). During the flood period, most vectors point to the central zone, which means the actual (sand ridge) topography centralized the radial currents. As a result, sediments transported to the central zone due to the actual topography. During the ebb tide, most vectors point to the coast line, which means the sediments transported to the coastal area due to the actual topography. So it can be concluded that, the actual topography stimulated the sediment transport to the central zone and the coastal area, providing sediments for reclamation projects.

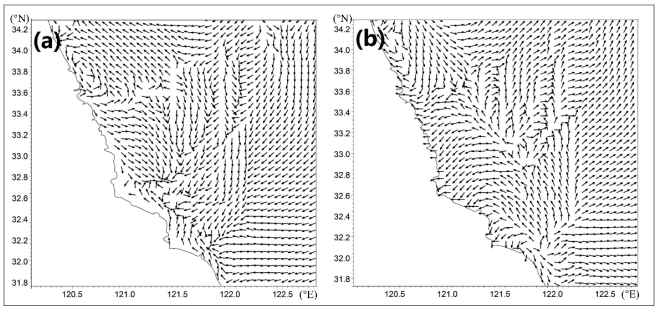

Fig. 7. Unit ATE in study area. (a) flood tide period; (b) ebb tide period

LAGRANGE RESIDUAL CURRENT

For the large-scaled circulation currents, the residual current is defined as the ratio of the water particle drift to the time period accordingly [12-14]. The process of the long-term mass transport depends on Lagrangian residual currents[15]. Therefore, the Lagrangian residual currents can be roughly analysed to present the sediment sources and transport routes (shown in Figure 8). The horizontal axis is the longitude (in °E), and the vertical axis is the latitude (in °N).

Figure 8(a) shows the Lagrangian residual currents are relatively simple on gradually changing topography. The residual currents near the coastline appear to be stronger than others. The residual current A travelled from the ancient Yellow River estuary towards south with the velocities of 0.12-0.16 m/s; the residual current B travelled from Yangtze River estuary towards north with the velocities of 0.1-0.18 m/s. Residual currents A and B converged in the central area and transformed into a circular residual current C with the velocities of 0.05-0.18 m/s. These results indicate that: 1) before the sand ridges were generated, the sediments were carried by residual currents; 2) the original source of the sediment could be either the ancient Yellow River estuary or Yangtze River estuary. This hydrodynamic finding is consistent with the environmental magnetism results [16] and the sediment composition results [17]. Once the sand ridges had been formed, the Lagrangian residual current varied (shown in

Figure 8(b)). The actual (sand ridge) topography weakened the external residual currents. As a result, the study area became a quasi-closed system without abundant sediment supply from outside. While in the sand ridges area several circular residual currents were generated with the velocities of 0.08-0.17 m/s. These residual currents transported and redistributed the sediments in this quasi-closed system.

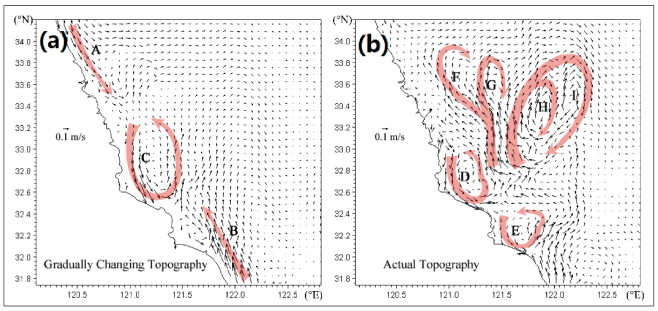

Fig. 8. Lagrangian residual currents in study area. (a) on gradually changing topography, the sediment transported to the study area; (b) on actual topography, no more sediment trans-ported to the study area, so it is a quasi-closed system.

CONCLUSIONS

In this study, field surveys were conducted to investigate the time-histories of tidal levels, current velocities and current directions in South Yellow Sea, China. Based on field data, a large-scaled numerical model was developed to simulate the radial current fields. Two parallel experiments were conducted on the actual topography and the gradually changing topography, respectively. The conclusions are drawn as follows:

(1) A unique radial current field is generated by dual-tide system rather than actual (sand ridge) topography.

(2) The actual (sand ridge) topography narrows the central zone of the radial current field, increases the flood velocities and decreases the ebb velocities.

(3) Actual topographic effect is proposed in this study. Results show that actual topography stimulates the sediments to be transported to the central zone and the coastal area.

(4) The observations of the Lagrangian residual currents show the sediments originally travel from the ancient Yellow River estuary or Yangtze River estuary. The actual (sand ridge) topography makes study area become a quasi-closed system.

ACKNOWLEDGEMENTS

The authors gratefully acknowledge the support of Fuzhou University scientific start-up expenses (No. 0050-510479), the National Key Technologies R&D Program of P. R. China (No. 2012BAB03B01), the Jiangsu Natural Science Foundation for the Youth (No. BK2012411), and the Cultivation and Innovation Project for Postgraduate in Jiangsu (No. CXZZ13_0258).

REFERENCES

1. Z. Liu, S. Berne, H. Yu, A. Trentesaux, K. Uehara, P. Yin, J. P. Liu, C. Li, G. Hu, 2007. Internal architecture and mobility of tidal sand ridges in the east china sea. Continental Shelf Research, 27 (13), 1820-1834.

2. K. R. Dyer, D. A. Huntley, 1999. The origin, classification and modelling of sand banks and ridges. Continental Shelf Research, 19 (10), 1285-1330.

3. C. Chen, Y. G. Wang, H. M. Huang, C. G. Yuan, 2013. Advancement in impacts of tidal dynamics on radial sand ridges. Port & Waterway Engineering, 8, 17-24. (in Chinese)

4. Y. G. Wang, C. Chen, H. M. Huang, 2012. Beach reclamation related issues of tiaozini in jiangsu. Zhejiang Hydrotechnics, 1, 4-7. (in Chinese)

5. Z. W. Xia, Z. J. Wang, H. M. Huang, 1984. Numerical model of the m2 constituent in the huanghai sea. J Oceanogr Hunghai Bohai Seas, 2 (1), 1-7. (in Chinese)

6. Y. R. Zhu, R. F. Chang, 1997. Explanation of the origin of radial sand ridges in the southern yellow sea with numerical simulation results of tidal currents. Journal of Ocean University of Qingdao, 27 (2), 218-224. (in Chinese)

7. C. Zhang, D. Zhang, Z. Wang, 1999. Tidal current-induced formation—storm-induced change—tidal current-induced recovery. Science in China Series D: Earth Sciences, 42 (1), 1-12.

8. D. Zhang, J. Zhang, 1996. M2 tidal wave in the yellow sea radiate shoal region. Journal of Hohai University, 24, 35-40. (in Chinese)

9. Y. Zhu, 1998. Numerical simulation of paleo-tidal current field in the subei littoral plain area and its verification. Marine Science Bulletin-Tianjin, 17, 7-13. (in Chinese)

10. K. Chen, P. Lu, Y. Wang, G. Yu, 2010. Hydrodynamic mechanism of evolvement trends in radial sandbank of south yellow sea, china. Advances in Water Science, 21 (2), 123-129. (in Chinese)

11. F. Xing, Y. P. Wang, H. V. Wang, 2012. Tidal hydrodynamics and fine-grained sediment transport on the radial sand ridge sys-tem in the southern yellow sea. Marine Geology, 291, 192-210.

12. M. S. Longuet-Higgins, 1969. On the transport of mass by time-varying ocean currents. Deep Sea Research and Oceanographic Abstracts (Elsevier), 16 (5), 431-447.

13. J. Zimmerman, 1979. On the euler-lagrange transformation and the stokes drift in the presence of oscillatory and

residual currents. Deep Sea Research Part A Oceanographic Research Papers, 26 (5), 505-520.

14. R. T. Cheng, V. Casulli, 1982. On lagrangian residual currents with applications in south san francisco bay, california. Water Resources Research, 18 (6), 1652-1662.

15. S. Feng, R. T. Cheng, X. Pangen, 1986. On tide-induced lagrangian residual current and residual transport: 1. Lagrangian residual current. Water Resources Research, 22 (12), 1623-1634.

16. C. Li, J. Zhang, S. Yang, D. Fan, 1999. Characteristic and paleoenvironmental evolution of subaerial tidal sand body in subei coastal plain. Science in China Series D: Earth Sciences, 42 (1), 52-60.

17. Y. Wang, Y. Zhang, X. Zou, D. Zhu, D. Piper, 2012. The sand ridge field of the south yellow sea: Origin by river–sea interaction Marine Geology, 291, 132-146.

CONTACT WITH THE AUTHOR

Cheng Chen

College of Civil Engineering
Fuzhou University
Fuzhou 350116
China